Materials Science & Engineering A 651 (2016) 763–773

Contents lists available at ScienceDirect

Materials Science & Engineering A

journal homepage: www.elsevier.com/locate/msea

Structural/textural changes and strengthening of an advanced high-Mn steel subjected to cold rolling

Z. Yanushkevich [a,b], A. Belyakov [a,*], C. Haase [b], D.A. Molodov [b], R. Kaibyshev [a]

[a] Belgorod State University, Pobeda 85, Belgorod 308015, Russia
[b] Institute of Physical Metallurgy and Metal Physics, RWTH Aachen University, 52056 Aachen, Germany

ARTICLE INFO

Article history:
Received 6 September 2015
Received in revised form
6 November 2015
Accepted 9 November 2015
Available online 12 November 2015

Keywords:
electron microscopy
mechanical properties
austenitic steel
twinning
texture
hardening.

ABSTRACT

The microstructure and texture evolution during cold rolling with total thickness reductions of 20–80% (nominal strains of 0.22–1.61) and their effect on the tensile behavior of an Fe–17Mn–1.5Al–0.3C steel were studied. The cold rolling to total strains of 0.5 was accompanied by multiple deformation twinning, resulting in the formation of twin/matrix lamellae with the boundary spacing of 35 nm. Correspondingly, the textural changes were characterized by the rapid evolution of rather strong Brass and S texture components. An increase in the rolling strain led to further reduction in the boundary spacing down to about 20 nm and the development of shear banding, which promoted the formation of γ-fiber (⟨111⟩||ND) at large strains. Before cold rolling, the investigated steel exhibited a large total elongation above 90% because of the TWIP (twinning-induced plasticity) effect and a relatively low yield strength of 245 MPa. The cold rolling resulted in significant increase in the yield strength up to 1440 MPa after rolling to a total strain of 1.61, whereas the total elongation decreased to 5%. The strengthening of the present steel during cold rolling was attributed to increased dislocation density and reduced twin/grain boundary spacing.

1. Introduction

Recently, high-Mn austenitic steels have aroused a great interest among materials scientists and mechanical engineers [1–5]. This interest is primarily motivated by an extraordinary strain hardening leading to outstanding ductility of high-Mn austenitic steels. Such an unusual deformation behavior is attributed to pronounced deformation twinning resulting in so-called twinning-induced plasticity (TWIP) effect [1,2]. The TWIP effect is expected in high-Mn austenitic steels, which have relatively low stacking fault energy (SFE) of 20–50 mJ/m^2 at ambient temperature [6,7]. Besides manganese, the TWIP steels are usually alloyed with carbon, aluminum and silicon to obtain the desired value of SFE. The excellent combination of strength and ductility of high-Mn TWIP steels makes them very attractive for various structural applications, especially, for automobile engineering, where the strength-ductility relationship is closely associated with passenger safety.

Presently, most of high-Mn austenitic TWIP steels are semi-products processed under conditions of hot working. The main disadvantage of the hot worked semi-products with recrystallized microstructures is their relatively low yield strength of about 200–400 MPa [1,8], which limits their applications in crucial structural elements. Therefore, specific attention of the current research efforts focuses on alternative processing technologies, which could be utilized for processing of high-Mn TWIP steels with enhanced strength properties. Several approaches are considered for the fabrication of advanced high-Mn TWIP steels. Those include cold or warm working [9–12] and combinations of cold working and annealing [13–15]. It has been shown that conventional high-Mn TWIP steels can be processed in a high strength state with the yield strength above 600 MPa and sufficient ductility, i.e., total elongation beyond 30% [9]. The cold rolling is the most efficient processing method that can be used for the development of high-Mn TWIP steels with beneficial combination of strength and ductility. The cold rolling results in the activation of deformation twinning and causes a drastic increase in the dislocation density, leading to significant strengthening. Shear banding follows deformation twinning at sufficiently large rolling strains that result in degradation of plasticity. In our recent studies [16–18] we investigated the correlation between microstructure and texture evolution during cold rolling. However, the influence of the microstructure evolution during cold rolling on the mechanical behavior is still not perfectly understood. In the preset study, the aim is to comprehensively investigate the structural and textural changes in an Fe–17Mn–1.5Al–0.3C austenitic steel during cold rolling with different rolling reductions and to clarify the

* Corresponding author.
E-mail address: belyakov@bsu.edu.ru (A. Belyakov).

http://dx.doi.org/10.1016/j.msea.2015.11.027
0921-5093/

structural/textural effect on the tensile properties of the cold worked material.

2. Experimental

A high-Mn austenitic TWIP steel containing 0.3 C, 17.7 Mn, 1.5 Al, 0.01 Si, 0.07 Cr, 0.007 S, 0.02 P (all in wt%) was investigated. The steel ingot was solution treated at 1150 °C for 4 h followed by hot forging from 140 mm to 50 mm thickness in 3 passes and subsequently annealed at 1150 °C for 4 h. The forged slab was hot rolled at an initial temperature of 1150 °C to 10 mm thickness and then annealed at the same temperature for 1 h. This thermo-mechanical treatment resulted in the formation of a uniform microstructure composed of equiaxed grains with an average size of 24 μm. The plate samples were cold rolled to 8, 6, 4 and 2 mm sheets (the rolling reductions are 20%, 40%, 60% and 80%; and the true strains are 0.22, 0.51, 0.91 and 1.61, respectively) at ambient temperature with a pass strain of about 0.1. The structural investigations were performed on the RD-ND sections (RD – rolling direction, ND – normal direction), using a Quanta 600 field emission gun scanning electron microscope (SEM) and Jeol JEM-2100/2000 FX II transmission electron microscopes (TEM). The SEM/TEM samples were electro-polished using an electrolyte composed of 10% perchloric acid and 90% acetic acid at a voltage of 20 V at room temperature. The deformation microstructures were revealed by etching at room temperature using an etching solution consisting of 2 g potassium disulfide ($K_2S_2O_5$) and 100 ml cold saturated Klemm I solution ($Na_2S_2O_3+5H_2O$). The misorientations among fine substructures were analyzed by the conventional TEM Kikuchi-line method with a converged beam technique [19]. The rolling textures were studied using a Bruker D8 Advance diffractometer with a HI-STAR area detector and polycapillary focusing optics. The orientation distribution functions (ODF) were calculated in MTEX using the data from three incomplete pole figures, i.e., {111}, {200}, {220}. Assuming a spread of 15° from the respective ideal orientation, the volume fractions of the various texture components were calculated. The dislocation densities were determined by X-Ray diffraction profile analysis using an ARL-Xtra diffractometer. The dislocation density (ρ) was calculated from the average values of the crystallite size (D) and the microstrain $\langle\varepsilon^2\rangle$, $\rho=3\ (2\pi)^{0.5}\ \langle\varepsilon^2\rangle/(Db)$, where b is the Burgers vector [20]. The tensile tests were carried out using an Instron 5882 testing machine on specimens with a gauge section of 1.5 mm × 3 mm cut out with the tensile direction parallel to the rolling direction.

3. Results

3.1. Deformation microstructures

The effect of rolling strain on the fraction of strain-induced ε-martensite is shown in Fig. 1 as revealed by X-Ray diffraction analysis. The cold rolling to a total strain of 0.22 (rolling reduction of 20%) is accompanied with a partial martensitic transformation, although the martensite fraction is small with about 2.9%. An increase in the rolling strain leads to a slight increase in the martensite fraction, which finally attains about 4.3% after rolling to a strain of 1.61 (80% reduction). Therefore, the austenite in the present steel is rather stable against strain-induced martesitic transformation.

Typical deformation microstructures that develop during cold rolling are shown in Fig. 2 The cold working is accompanied by extensive deformation twinning. Original grains are flattened by cold rolling and crossed over by twin bundles with at submicron

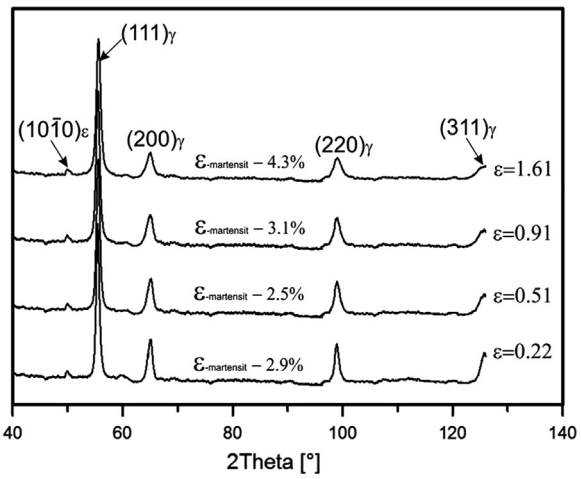

Fig. 1. X-Ray diffraction patterns of the Fe–17Mn–1.5Al–0.3C steel samples subjected to cold rolling to strains of ε=0.22 to ε=1.61.

scale level after rolling to a strain of 0.22 (Fig. 2a). The twin density and the number of activated twin systems increase with increase in the rolling strain. Up to three twinning systems were activated in some grains. The twin spacing reduces down to nanometer range as the rolling strain increases to 0.51. Another important feature of the deformation microstructure that evolves during cold rolling to a strain of 0.51 is the appearance of microshear bands, which cross over the twinned grains (Fig. 2b). The number of microshear bands and their thickness increase upon further cold rolling (Fig. 2c and d), whereas the twin/matrix lamellae tend to align with the rolling plane.

Fig. 3 shows the deformation substructures that evolve in the steel subjected to cold rolling to a total strain of 0.22. Generally, the deformation substructures are characterized by high dislocation densities beyond 10^{15} m^{-2}. Individual dislocations are hard to be resolved by conventional TEM observations. The primary (relatively thick) and secondary (thin) deformation twins are clearly seen in Fig. 3. The average spacing between twin boundaries is 190 nm. The image of the deformation twins appear at the transverse section of the rolled sample at about 20° to 60° to the rolling plane in Fig. 3. The formation of ε-martensite phase occurs rarely as proved by the dark-field image in Fig. 3c. It is interesting to note that the ε -martensite plates look like the secondary deformation twins. Probably, the ε-martensite nucleates at secondary deformation twins along the same close packed crystallographic austenite plane. The lettered points in Fig. 3b indicate the portions of primary twins, where the local crystallographic orientations were evaluated by converged beam Kikuchi-line technique. In spite of large internal distortions caused by high dislocation density, twining, and martensitic transformation, the primary twins retain their crystallographic relationships close to ideal ones. The deviations of the measured misorientations (Fig. 3b) from the ideal Σ3 twin boundaries are 2.5° and 1.0° for A–B and B–C points, respectively.

The twin density increases substantially with an increase in the rolling strain to 0.51 (Fig. 4). The multiple deformation twining results in the development of complex microstructures composed of frequently intersected twins belonging to different twinning systems (Fig. 4a). Correspondingly, the average twin boundary spacing on the transverse section decreases to 35 nm. The development of nano-lamellar structure is a prerequisite for microshear banding. Fig. 4b shows details of a microshear band, which passes over a grain and shear the nano-twinned lamellae. The microshear band appears at about 45° to the rolling plane as a narrow region (about 100 nm in thickness) of localized shear that oriented with

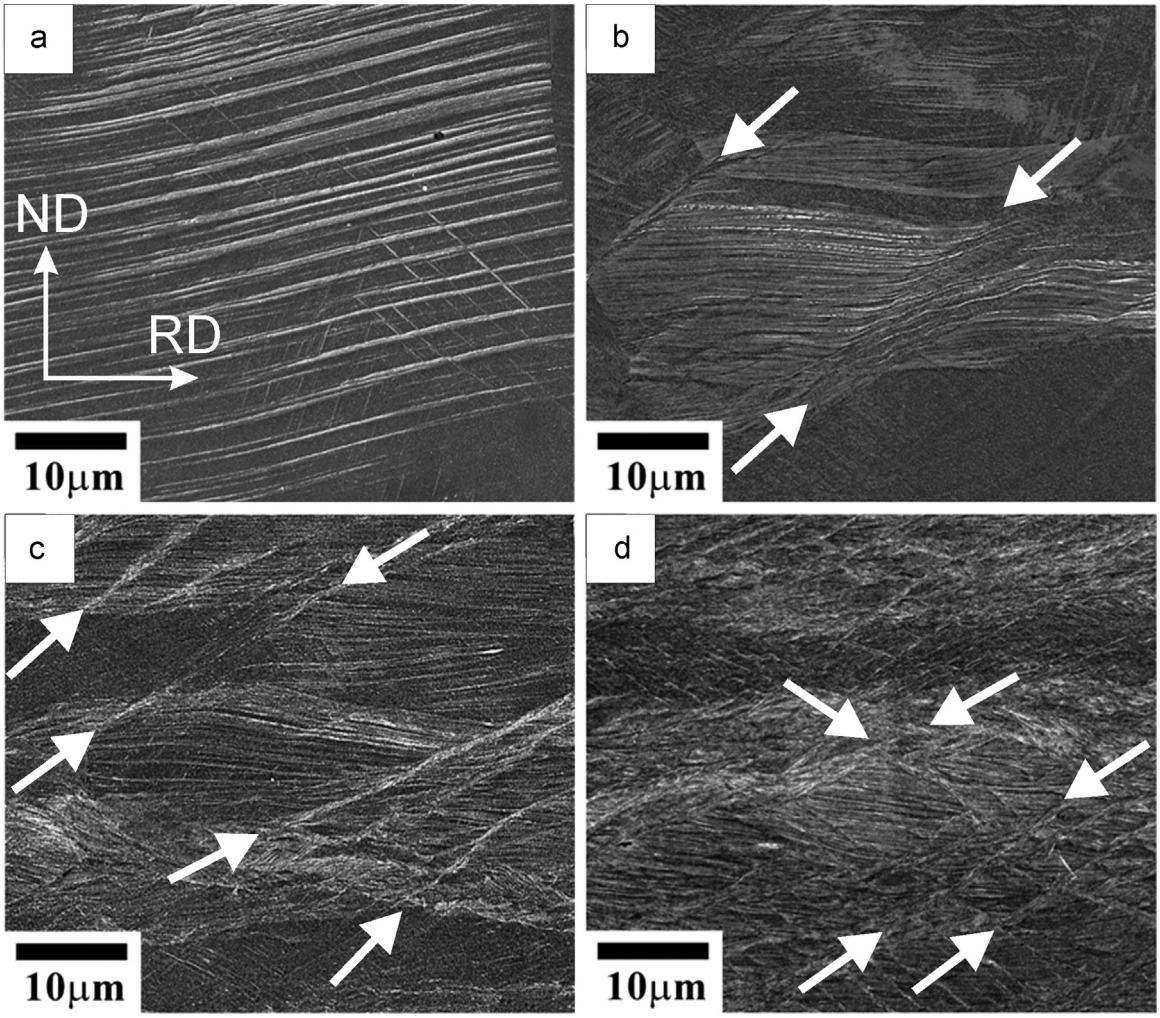

Fig. 2. Optical micrographs of the Fe–17Mn–1.5Al–0.3C steel subjected to cold rolling to total strain of 0.22 (a), 0.51 (b), 0.91 (c), and 1.61 (d). The white arrows indicate microshear bands.

⟨111⟩||ND and ⟨011⟩||RD (Fig. 4b). It should be noted that this orientation corresponds to so-called E texture component, which has been frequently observed in high-Mn steels subjected to large strain cold rolling [14–17].

Further rolling to large total strains is accompanied by frequent development of microshear bands. Numerous crossing microshear bands appear on the TD plane at about $\pm 35^\circ$ to the rolling plane in the steel samples rolled to a total strain of 0.91 (Fig. 5a). The thickness of microshear bands increases with increasing the rolling strain. It is clearly seen in Fig. 5b that the microshear band consists of ultrafine crystallites, which are somewhat elongated along the shear direction. The thickness of individual microshear bands attains 500 nm after a total rolling strain of 1.61 (Fig. 6a). It is worth noting that the microshear bands locate at larger angles to the rolling plane than the twin planes at large strains (Fig. 2d and 6a). The deformation substructures that develop in the steel samples subjected to large strain cold rolling are characterized by large internal distortions. Nevertheless, the twins retain their ideal relationship even after such a large cold strain as 1.61. For instance, the deviation from the ideal twin misorientation for the lettered points of A and B in Fig. 6b is 1.4°. This suggests that the reorientation of twin lamellae along the rolling plane occurs like rigid body rotation without significant deformation within the rotated microvolume. On the other hand, the local disorientation between two nano-regions located within a twin/matrix lamella may comprise rather large angles (e.g. 3° between B and C in Fig. 6b) that is indicative of large internal distortions, which can be attributed to the high dislocation density. It is worth noting that the disorientation direction in Fig. 6b is close to ⟨101⟩ that corresponds to the stored dislocations with total Burgers vector along ⟨211⟩. This may result from Shockley partials (i.e., b=1/6[211]) or combination of two dislocation families (e.g., b_1=1/2[110] and b_2=1/2[101]).

The effects of cold rolling strain on the twin boundary spacing and the dislocation density are shown in Fig. 7. The twin boundary spacing rapidly reduces to tens of nanometers during cold rolling to a strain of about 1, and then scarcely changes during subsequent rolling. The dashed lines in Fig. 7a indicate the change in the transverse size of any elements/features of microstructure in accordance with the sample thickness reduction. The boundary spacing decreases much faster than could be expected from the rolling reduction in the strain range of $\varepsilon\langle 0.5$. In contrast, the rolling reduction does not affect the boundary spacing, which seems to be almost strain invariant, in the strain range of $\varepsilon\rangle 0.5$. It can be concluded, therefore, that the deformation twinning frequently operates in the present steel during cold rolling to a total strain of approx. 0.5, and that is exhausted at larger strains. On the other hand, the microshearing can provide the plastic deformation without remarkable change in the boundary spacing, which becomes unchanged when the microshear banding develops at large rolling strains. Contrary to bimodal strain dependency for the twin boundary spacing, the dislocation density exhibits monotonous

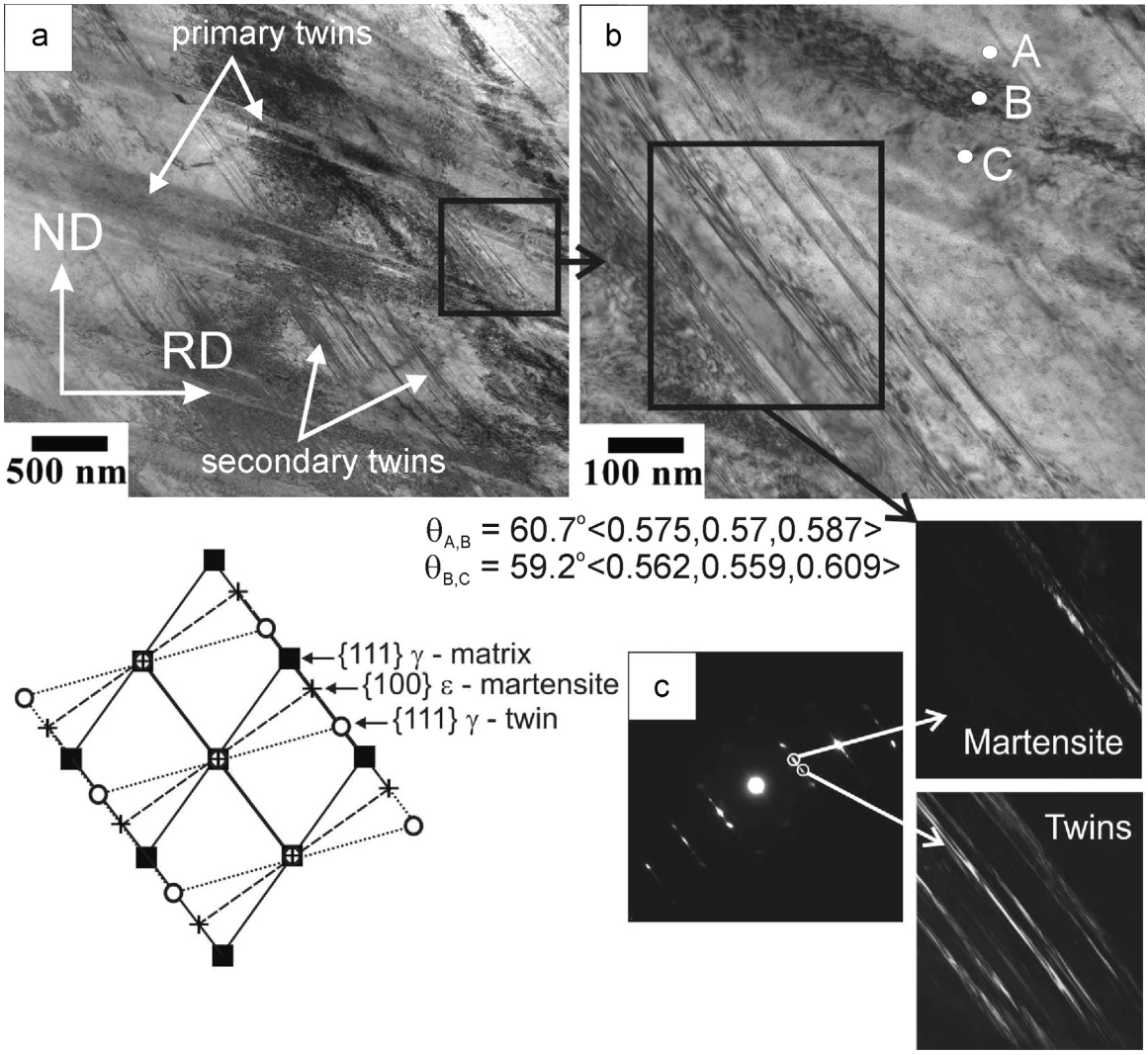

Fig. 3. TEM bright field (BF) images (a), (b) and diffraction pattern with corresponding dark field images (c) of deformation microstructure of the Fe–17Mn–1.5Al–0.3C steel subjected to cold rolling to a total strain of 0.22. The misorientations correspond to the lettered points in (b).

increase with straining (Fig. 7b). This suggests progressive strengthening of the steel during cold rolling.

3.2. Rolling textures

The representative orientation distribution functions (ODF) for the samples subjected to cold rolling to various total strains are shown in Fig. 8a. The main texture components that appear in fcc steels are shown in Fig. 8b and defined in Table 1. Generally, the deformation textures are characterized by the development of α- and γ-fibers, i.e., ⟨110⟩∥ND and ⟨111⟩∥ND, respectively. The α-fiber with a maximum corresponding to Brass texture component, {110}⟨112⟩, rapidly develops at an early stage of deformation (cf. ODF at $\varepsilon=0.22$ in Fig. 8a). Further rolling to large total strains is accompanied by a slight strengthening of α-fiber, while the maximum corresponding to Brass texture gradually shifts towards the Goss texture component, {110}⟨100⟩ (cf. ODF at $\varepsilon=0.51$ and $\varepsilon=1.61$ in Fig. 8a). On the other hand, the γ-fiber appears at large rolling strains.

The variation of the volume fractions of different texture components during cold rolling is represented in Fig. 9. The cold rolling to total strains of about 0.5 results in the development of rather strong Brass and S ({123}⟨634⟩) texture components; their volume fractions attain 0.15 and 0.1, respectively. It should be noted that further cold rolling to large rolling strains does not lead to any remarkable changes in the fractions of these texture components. In contrast, cold rolling to strains above 0.5 leads to the development of E ({111}⟨110⟩) and F ({111}⟨112⟩) texture components, whose fractions progressively increase in the strain range of $\varepsilon\rangle 0.5$, exceeding 0.05 at $\varepsilon=1.61$. The development of E and F texture components belonging to γ-fiber is evidently associated with the microshear banding at large rolling strains (s. Fig. 4). Also, cold rolling within the studied strain range of $0\langle\varepsilon\langle 1.61$ is characterized by a gradual increase of the volume fractions of Copper-twin ({112}⟨111⟩) and Goss texture components, which finally approach 0.09 and 0.07, respectively.

3.3. Tensile behavior

The engineering and true stress–strain curves obtained for the steel samples by tensile tests at ambient temperature are shown in Fig. 10a and b, respectively. The true stresses were calculated assuming uniform reduction of cross sections of specimens until fracture. The initial, hot rolled, steel ($\varepsilon=0$) exhibits pronounced strain hardening leading to increase of the true tensile stress from 245 MPa (yield point) to 1355 MPa (maximal stress at a true tensile strain of 0.63). Correspondingly, the total elongation and uniform elongation comprise 96% (true strain of 0.67) and 88%

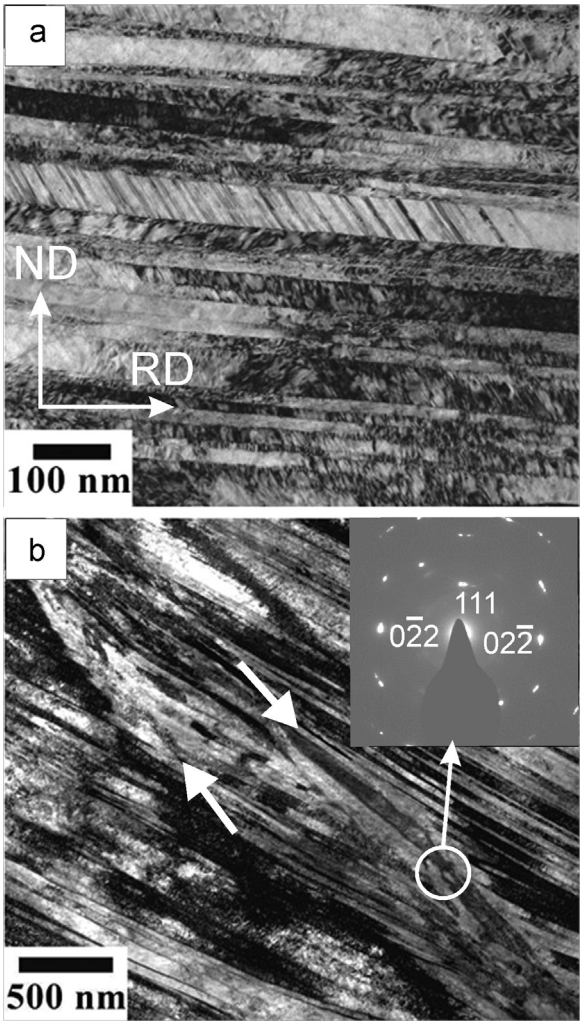

Fig. 4. TEM BF images showing the multiple deformation twinning (a) and the microshear bands (b) in the Fe–17Mn–1.5Al–0.3C steel sample subjected to cold rolling to a total strain of 0.51. The white arrows indicate the microshear bands crossing over the twin/matrix lamellae.

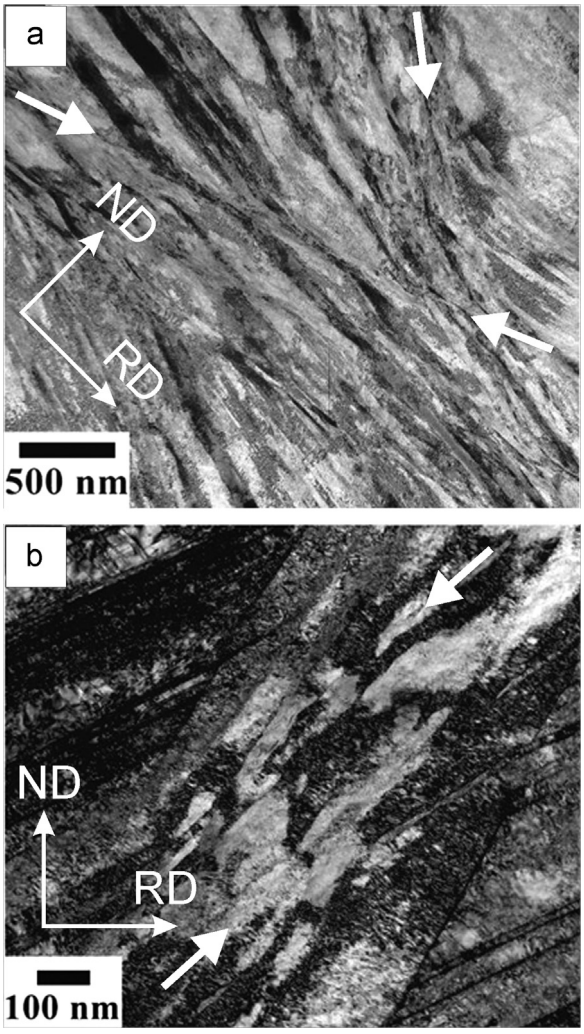

Fig. 5. TEM BF images showing the deformation microstructures in the Fe–17Mn–1.5Al–0.3C steel sample subjected to cold rolling to a total strain of 0.91. The white arrows indicate the microshear bands.

(true strain of 0.63), respectively. The cold rolling results in significant strengthening of the steel. The yield strength progressively increases from 790 MPa to 1440 MPa with increase of the rolling reduction from 20% to 80% ($\varepsilon=0.22$ to $\varepsilon=1.61$ in Fig. 10a). Note here that the strengthening by cold rolling is accompanied by drastic degradation of plasticity.

The shape of true stress–strain curve significantly depends on the previous rolling strain (Fig. 10b). The tensile behaviors of the initial (hot rolled) steel sample and the steel sample subjected to cold rolling to a strain of 0.22 are characterized by remarkable strain hardening leading to almost linear increase in the true stress with tensile strain. On the other hand, the tensile behavior of the steel samples previously cold rolled to strains of $\varepsilon\rangle 0.5$ is quite different to that typically inherent to annealed (recrystallized) high-Mn TWIP steels. Namely, the true flow stress quickly attains its maximum just after yielding followed by necking and failure. This difference in the tensile behavior between the steel samples cold rolled to strains of below or above 0.5 suggests that the TWIP effect in the present steel takes place during deformation up to true strains of approx. 0.5. The same conclusion can be drawn from the structural analysis, which suggests the strain level of about 0.5 being a separating point between the deformation twinning and the microshear banding.

4. Discussion

4.1. Regularities of microstructure and texture evolution

The microstructure evolution in the present high-Mn TWIP steel during cold rolling is typical for fcc metals/alloys with low SFE. Namely, the structural changes are characterized by the development of deformation twins at small to moderate strains followed by microshear banding at large strains. In the present steel, the deformation twinning readily occurs in the strain range of approx. $0\langle\varepsilon\langle 0.5$, resulting in the development of layered twin/matrix microstructure with nanoscale spacing between the boundaries. The twin boundary spacing depends on twinning, i.e. new twin formation, whereas the rolling reduction has a negligibly small effect on the thickness of twin/matrix lamellae. This statement holds for both the range of small to moderate strains, when the deformation twinning rapidly develops leading to drastic decrease in the boundary spacing, and the range of large strains, when the deformation twinning scarcely takes place and, therefore, the boundary spacing does not change with straining (Fig. 7). It should also be noted that the strain invariant boundary spacing at large strains suggests that the plastic flow takes place locally within microshear bands, while the islands of twin/matrix lamellae, which locate between the microshear bands, experience quite small homogeneous deformation.

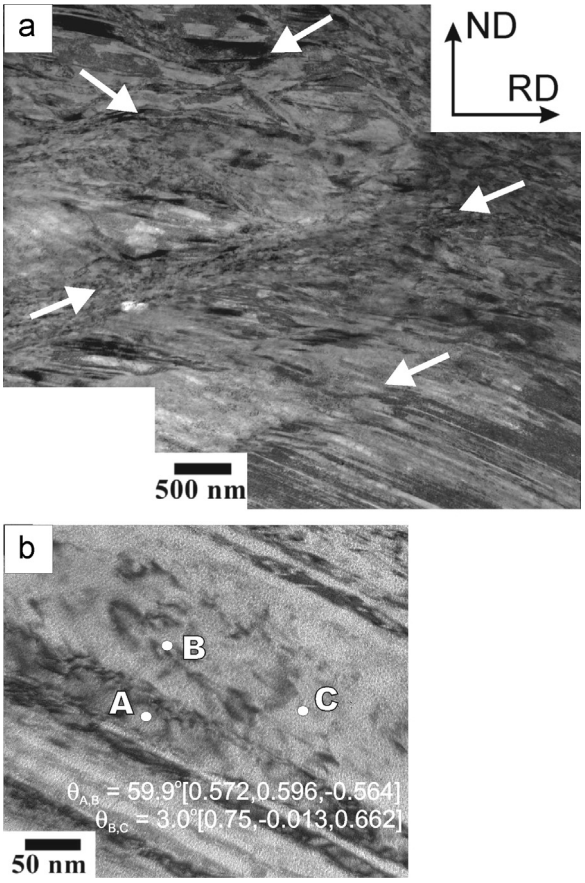

Fig. 6. TEM BF images showing the microshear bands (indicated by white arrows in (a)) in the Fe–17Mn–1.5Al–0.3C steel sample after cold rolling to a strain of 1.61. The misorientations in (b) corresponds to the lettered areas in twin/matrix lamellae.

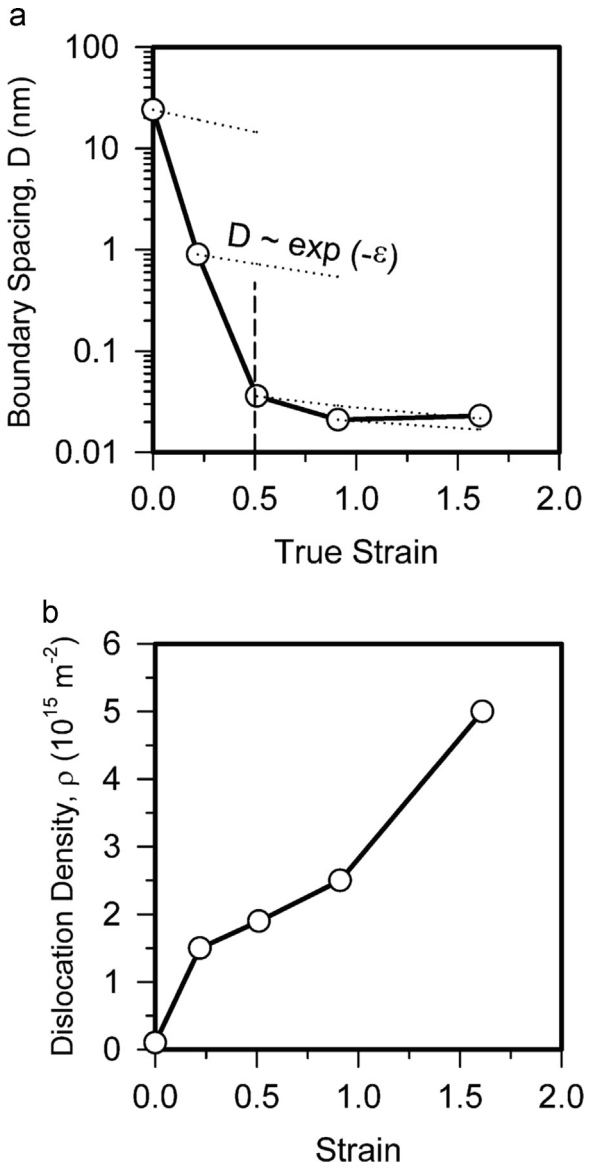

Fig. 7. Effect of the degree of cold rolling on the twin boundary spacing (a) and dislocation density (b) in the Fe–17Mn–1.5Al–0.3C steel.

The textures that develop during cold rolling are closely related to the microstructural changes. Generally, the rolling textures in fcc metals/alloys consist of an orientation tube with a skeleton line stretching along the β-fiber, ⟨110⟩ tilted 60° from ND to RD, from the Copper texture component, {112}⟨111⟩, over the S to the Brass texture component followed by the α-fiber [21]. The orientation density along the tube depends on concurrent operations of dislocation slip, deformation twinning and shear banding, these contributions, in turn, depend on the SFE. A decrease of SFE promotes the development of deformation twinning followed by shear banding and, therefore, leads to reduction of the intensity of the Copper texture component; correspondingly, the volume fraction of the Brass texture component increases [22,23].

The texture in the present steel can be characterized by a rapid development of rather strong Brass and S texture components, and a Copper-twin texture component, which strengthens with rolling strain (Fig. 9), that is typical of cold rolled low SFE fcc materials susceptible to deformation twinning and shear banding [16,17,24–26]. Probably, the amount of ε-martensite is not enough to affect the texture evolution remarkably. Examples of the major texture components are schematically shown in Fig. 11. Here, the planes, (hkl), are indicated by their normals. The dislocation slip and deformation twinning at small to moderate rolling strains (ε⟨0.5) result in the development of Brass and S components. Upon further cold rolling the deformation twinning stops and the microshear banding starts to operate. Correspondingly, the Brass and S orientations/components approach their saturation and do not vary during subsequent rolling. On the other hand, the E and F texture components start to develop at relatively large rolling strains of ε⟩0.5. An example of E component, which is almost the same with that experimentally observed for the microshear band in Fig. 4b, is also schematically shown in Fig. 11. It is worth noting that the E texture component developed in shear bands can be considered as a Brass texture component with respect to the microshear band plane (Fig. 11).

The twin/matrix lamellae and corresponding {111} planes rotate into the rolling plane during cold rolling. As a consequence, slip on these planes becomes very difficult and shear banding is activated. The shear bands have been considered as non-crystallographic bands that appear macroscopically at about 45° to the rolling plane [22]. At a nucleation stage, however, the microshearing should be associated with a cooperative dislocation slip. The S texture component seems to be preferable orientation for the microshear band nucleation, because it includes {111} planes inclined with about 50° to the rolling plane (Fig. 11). The S texture component fraction slightly decreases when the microshear bands develop (Fig. 9). The same results have been reported in other studies on rolling textures in high-Mn steels [14–17]. The development of microshearing within other developed textural components, e.g., Brass and Copper-twin, may be possible with an assumption that shear propagates along non-close packed planes

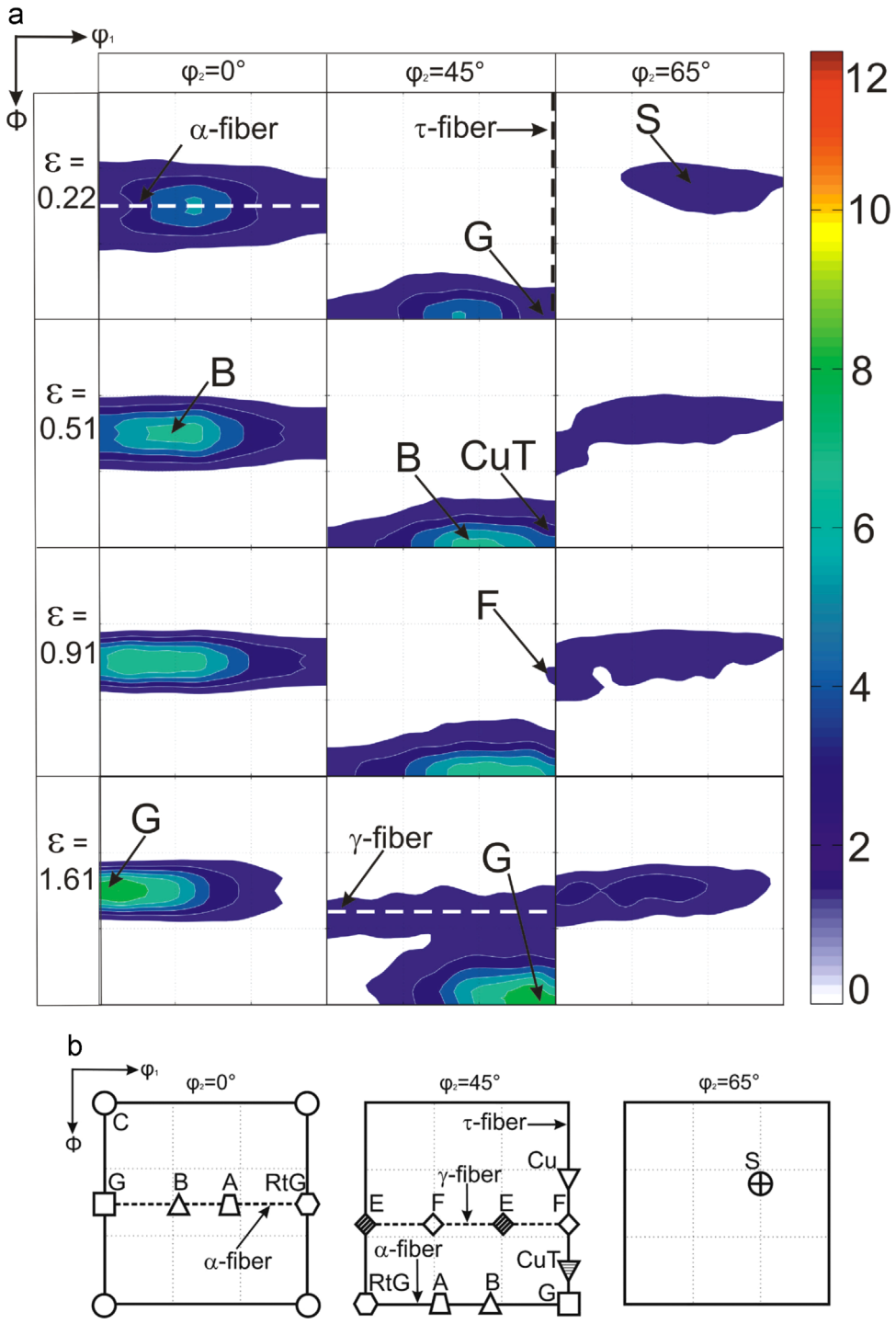

Fig. 8. ODF sections ($\varphi_2=0°$, $\varphi_2=45°$, $\varphi_2=65°$) of Fe–17Mn–1.5Al–0.3C steel samples subjected to cold rolling, (a) experimental and (b) schematic.

like {112}, which are located at 55° or 39° to the rolling plane in the Brass or Copper-twin texture components, respectively (Fig. 11). The developed microshear band experiences reorientation of its volume towards some stable orientation with respect to the shear plane, e.g., Brass-type component in Fig. 11. Thus, the microshear band can be oriented with ⟨111⟩||ND, that is the γ-fiber with respect to the rolled sample, and the shear direction between ⟨110⟩ and ⟨112⟩, which are essentially the E and F orientations. The gradual increase of the fractions of Copper-twin and Goss texture components (Fig. 9) can be attributed to dislocation slip in microshear bands and twin/matrix lamellae [22]. In fact, simultaneous operation of two dislocation families as suggested by disorientation direction in twin/matrix lamellae in Fig. 6b should promote the development of Copper-twin texture component. On the other hand, the concurrent development of the Brass, Copper-twin and Goss texture components is responsible for the texture peak located on the α-fiber in the respective ODF sections in Fig. 8 ($\varepsilon=1.61$, $\varphi_2=0°$ and $\varphi_2=45°$).

4.2. Strengthening mechanisms

The cold rolling results in significant strengthening of the present steel. The steel samples subjected to cold rolling are characterized by high density of grain/twin boundaries and high

Table 1
Definition of texture components.

Component	Symbol	Miller Indices	Euler Angels (φ_1,Φ,φ_2)	Fiber
Brass (B)	△	{110}<112>	(55, 90, 45)	α, β
Goss (G)	□	{110}<100>	(90, 90, 45)	α, τ
Rotated Goss (RtG)	⬡	{110}<110>	(0, 90, 45)	α
A	⏢	{110}<111>	(35, 90, 45)	α
Cube (C)	○	{001}<100>	(45, 0, 45)	/
E	◈	{111}<110>	(0/60, 55, 45)	γ
F	◇	{111}<112>	(30/90, 55, 45)	γ
Copper (Cu)	▽	{112}<111>	(90, 35, 45)	β, τ
Copper Twin (CuT)	⩛	{552}<115>	(90, 74, 45)	τ
S	⊕	{123}<634>	(59, 37, 63)	β
α-fiber	<110> parallel to ND			
γ-fiber	<111> parallel to ND			
τ-fiber	<110> parallel to TD			

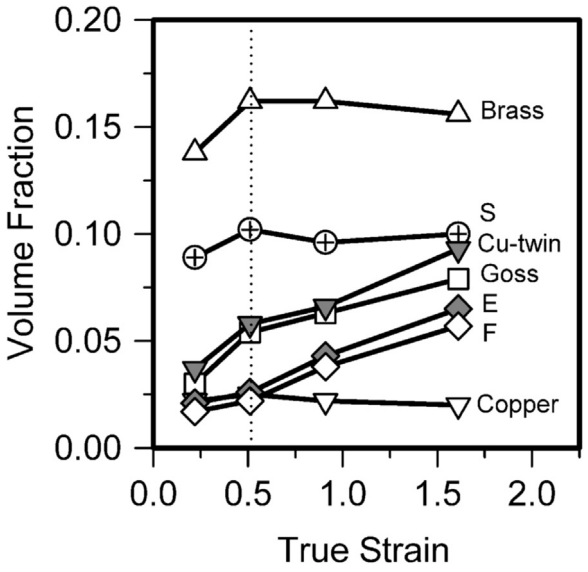

Fig. 9. Influence of cold rolling degree on the variations of the volume fractions of the main texture components in the Fe–17Mn–1.5Al–0.3C steel.

dislocation density. Both the grain/twin boundaries and the dislocation densities may strengthen the steel. Several approaches have been used by different researchers to obtain the structure-property relationship for largely strained metals/alloys. The strengthening of metallic materials processed by large strain deformation is commonly discussed in terms of grain boundary strengthening [27] or dislocation strengthening [28,29] or superposition of boundary and dislocation strengthening [30–32]. In the latter case, both the grain boundary strengthening and the dislocation strengthening are assumed to contribute independently to the overall strength. The grain boundary strengthening can be evaluated as

$$\sigma_{GB} = K_{\varepsilon} D^{-0.5} \quad (1)$$

where D is the grain size (boundary intercept length) and K_{ε} is a constant, and the dislocation strengthening is related to a square root of dislocation density as

$$\sigma_{DISL} = \alpha G b \rho^{0.5} \quad (2)$$

where α, G, and b are a constant, the shear modulus, and the Burgers vector, respectively.

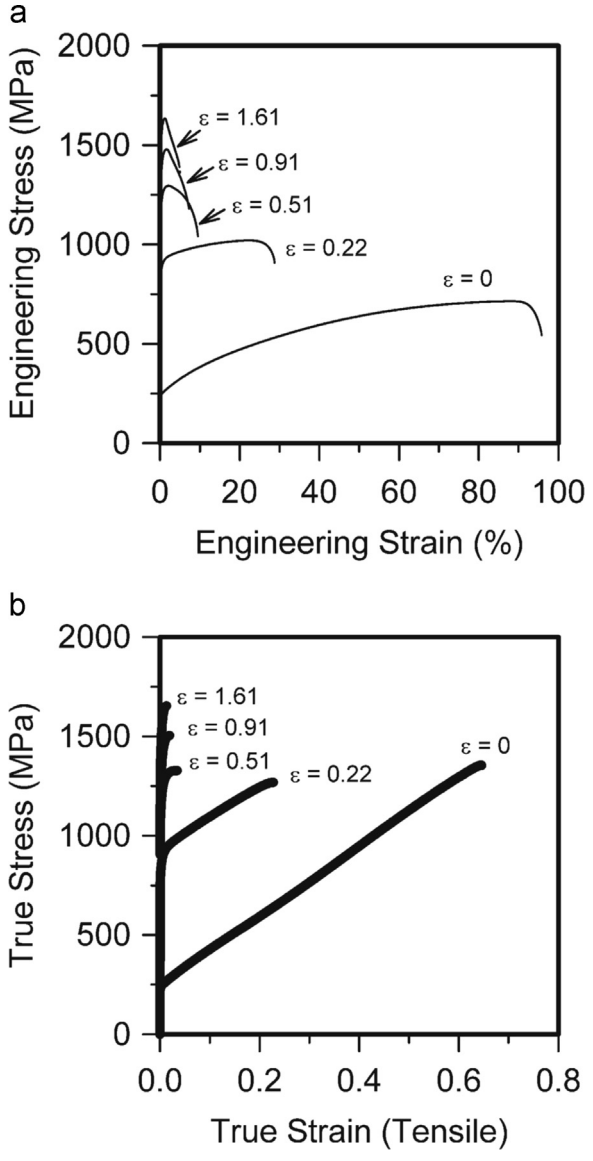

Fig. 10. Engineering (a) and true (b) stress – strain curves obtained by tensile tests of the Fe–17Mn–1.5Al–0.3C steel processed by cold rolling to various strains (ε).

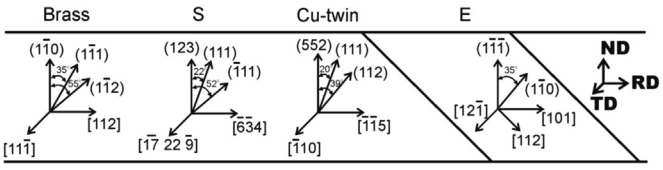

Fig. 11. Schematic representation of relatively strong texture components that develop in twin/matrix lamellae (Brass, S and Cu-twin) and within shear band (E) in the Fe–17Mn–1.5Al–0.3 C steel during cold rolling. The planes, (hkl), are indicated here by their normals.

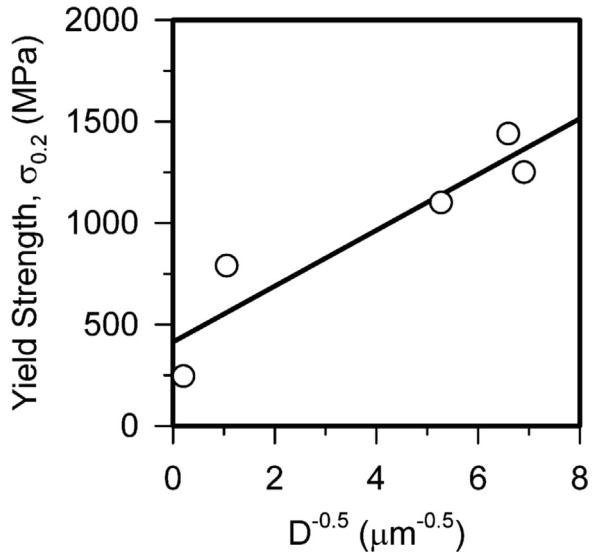

Fig. 12. Relationship between the yield strength and inverse square root of the boundary spacing for the Fe–17Mn–1.5Al–0.3C steel subjected to cold rolling. The straight line represents the linear fit of experimental points.

The plots of experimental $\sigma_{0.2}$ vs $D^{-0.5}$ and $\sigma_{0.2}$ vs $\rho^{0.5}$ are shown in Figs. 12 and 13, respectively. It is clearly seen in Fig. 12 that the relationship between the $\sigma_{0.2}$ and $D^{-0.5}$ demonstrates complex non-monotonous dependence, which cannot adequately be represented by a linear function. In contrast, the relationship between $\sigma_{0.2}$ and $\rho^{0.5}$ can be expressed as follows (Fig. 13):

$$\sigma_{0.2} = \sigma_0 + \alpha G b \rho^{0.5} \quad (3)$$

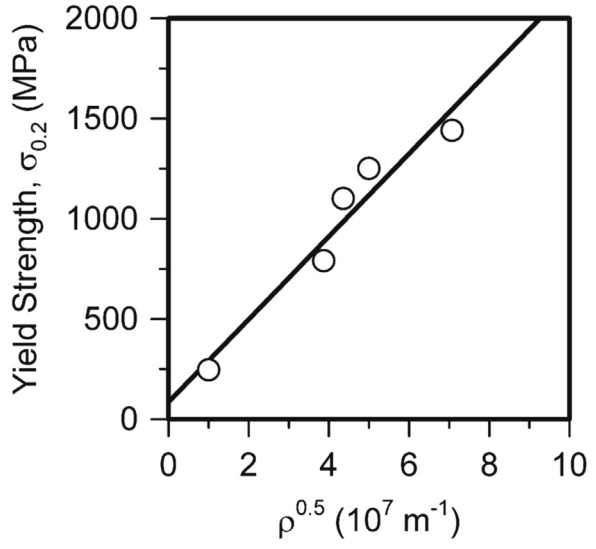

Fig. 13. Relationship between the yield strength and square root of the dislocation density for the Fe–17Mn–1.5Al–0.3C steel subjected to cold rolling. The straight line represents the linear fit of experimental points.

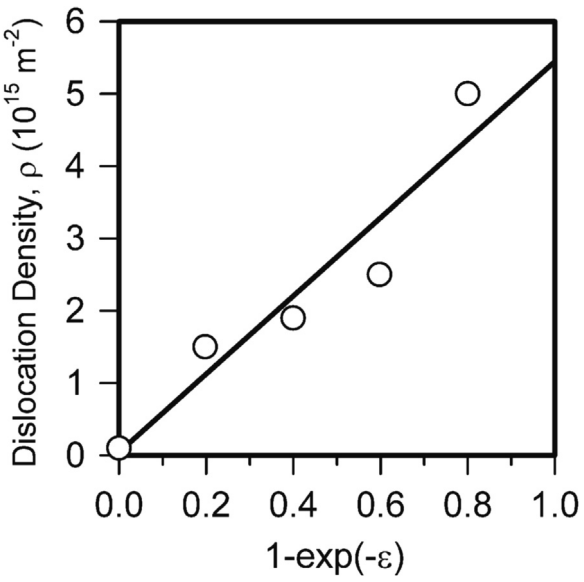

Fig. 14. Effect of cold rolling strain on the dislocation density in the Fe–17Mn–1.5Al–0.3C steel. The straight line represents the linear fit of experimental points.

where $\sigma_0 = 85$ MPa and $\alpha = 1$. Note here that a numerical factor, α, of 0.7 to 1.5 is commonly used for calculation of strength increments associated with dislocation density [14,30,33–35]. Therefore, the strengthening of the high-Mn TWIP steel subjected to cold rolling can be explained by an increasing dislocation density.

The change in the dislocation density during cold working has been suggested to obey an exponential function of true strain, $\Delta\rho \sim 1 - \exp(-\varepsilon)$ [36]. The relationship between the experimental dislocation density (ρ) and $(1 - \exp(-\varepsilon))$ is represented in Fig. 14. The experimental data for dislocation density in Fig. 14 can be expressed by the following equation:

$$\rho = \rho_0 + \beta(1 - exp(-\varepsilon)) \quad (4)$$

with $\rho_0 = 4.5 \times 10^{13}\ m^{-2}$ and $\beta = 5.4 \times 10^{15}\ m^{-2}$. Assuming the dislocation density being the major strength contributor, the yield strength can be calculated using Eqs. (3) and (4) for the steel samples, which were cold rolled to various strains. The experimental and calculated values of the yield strength are shown in Fig. 15 by open circles and solid line, respectively. It is clearly seen in Fig. 15 that the calculated yield strengths are quite coincident with the experimental ones.

Alternatively, the yield strength of cold rolled samples can also be expressed taking into account concurrent contributions from the grain/twin boundaries (Eq. (1)) and the dislocation density (Eq. (2)):

$$\sigma_{0.2} = \sigma_0 + K_\varepsilon D^{-0.5} + \alpha G b \rho^{0.5} \quad (5)$$

The best fit of experimental results is obtained when $\sigma_0 = 150$ MPa, $K_\varepsilon = 0.06$ MPa $m^{0.5}$, and $\alpha = 0.67$ as shown in Fig. 15 by dashed line. This approach predicts reasonable value for dislocation strengthening factor, $\alpha = 0.67$, which is close to that frequently used to evaluate the work hardening of various metallic materials. However, the grain boundary strengthening constant, $K_\varepsilon = 0.06$ MPa $m^{0.5}$, seems to be very small. Similar results have been obtained in other studies on austenite strengthening by large strain deformation, suggesting that dislocation strengthening provides the main contribution to the overall strength [9,32,37]. The significant strengthening effect from grain boundaries has been reported for ultrafine grained materials processed by severe plastic deformation [34]. The grain boundaries in these materials were considered being in non-equilibrium state that arouse high

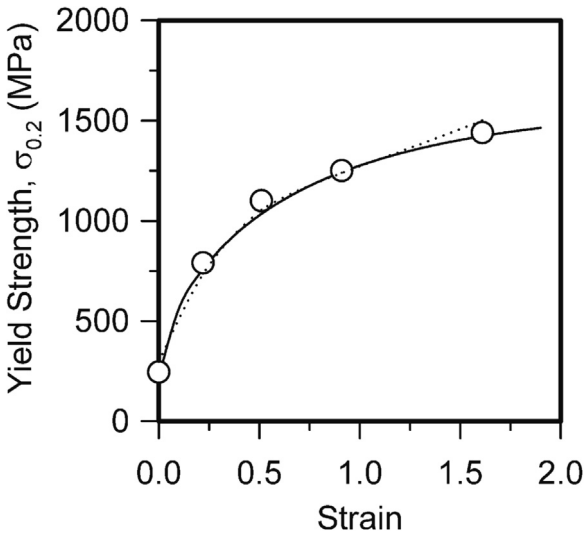

Fig. 15. Effect of cold rolling strain on the yield strength of the Fe–17Mn–1.5Al–0.3C steel. The symbols indicate the experimental data obtained by tensile tests, whereas solid and dotted lines correspond to those calculated by Eqs. (3) or (5), respectively.

internal stresses affecting the dislocation motion and, therefore, the strength of material [38,39]. In the present study, the dislocation densities were estimated by X-Ray diffraction, which actually evaluates the mean internal elastic distortions irrespective of their origin, i.e. those associated with lattice dislocations and grain boundary dislocations, including twin/matrix lamellae and microshear bands. Therefore, the strengthening of the present steel can be evaluated by either Eq. (3) or Eq. (5), because both of them make the dislocation density (namely, internal stresses) as the primary source of strengthening.

The deformation twinning provides a homogeneous increase of dislocation density up to some upper limit in a whole strained sample. It is worth noting that the hot rolled and cold rolled steel samples exhibit the same level of twinning-controlled strengthening (Fig. 16), similar to other high-Mn TWIP steels [9, 13-15, 40]. The maximal true tensile stress in the samples previously cold rolled to strains of $\varepsilon \leq 0.5$ (just before microshear band expansion) comprises about 1300 MPa. This strength level can be considered as an upper limit for twinning-controlled strengthening. Further strengthening can be achieved by subsequent cold rolling to large strains. The work hardening due to large strain deformation results in gradual strengthening above the twinning-controlled limit. The maximal true stress increases up to 1650 MPa as the previous rolling strain increases to 1.61 (Fig. 16). However, the large strain cold rolling is accompanied by the shear banding, which becomes essential feature of the deformation structure and results in a drastic degradation of plasticity in the samples cold rolled to strains of above 0.5.

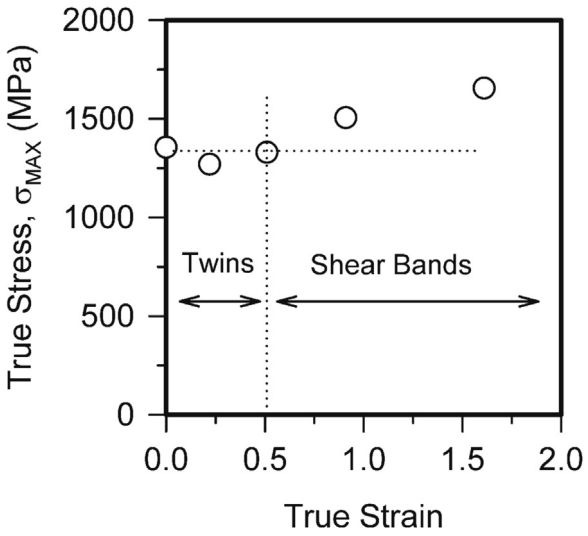

Fig. 16. Effect of cold rolling strain on the maximal true stress, which was attained by the tensile tests of the Fe–17Mn–1.5Al–0.3C steel.

5. Conclusions

The effect of cold rolling on the microstructure and texture evolution and strengthening of an advanced high-Mn austenitic TWIP steel was studied. The main results can be summarized as follows.

1. The structural changes during cold rolling were characterized by the development of deformation twinning at rolling strains up to about 0.5 followed by microshear banding upon subsequent rolling. The twin boundary spacing quickly decreased to 35 nm during cold rolling to a strain of 0.5 followed by further gradual decrease to about 20 nm at large strains. The cold rolled microstructure that developed at large strains consisted of twin/matrix lamella islands surrounded by microshear bands and involved high dislocation density. An increase in the dislocation density during cold rolling could be expressed by the following function of rolling strain:

$$\rho = \rho_0 + \beta(1 - exp(-\varepsilon))$$

where $\rho_0 = 4.5 \times 10^{13}$ m^{-2} and $\beta = 5.4 \times 10^{15}$ m^{-2}.

2. The deformation textures that developed during cold rolling at relatively small strains below about 0.5 were characterized by the evolution of rather strong Brass and S texture components. Further rolling was accompanied by the development of Copper-twin texture component. The development of microshear banding at large strains promoted formation of the γ-fiber texture components, namely the E and F orientations.

3. The hot rolled steel exhibited a large total elongation above 90% and a relatively low yield strength of 245 MPa. Cold rolling resulted in significant increase in the yield strength up to 1440 MPa after rolling to a total strain of 1.61. The strengthening of the present steel during cold rolling was attributed to an increase in the dislocation density and a reduction in the grain/twin boundary spacing. The yield strength could be expressed as:

$$\sigma_{0.2} = \sigma_0 + K_\varepsilon D^{-0.5} + \alpha G b \rho^{0.5}$$

where $\sigma_0 = 150$ MPa, $K_\varepsilon = 0.06$ MPa m$^{0.5}$, and $\alpha = 0.67$, suggesting that the dislocation density is a major contributor to the strengthening.

Acknowledgments

The authors acknowledge with gratitude the financial support received from the following sources: the Ministry of Education and Science, Russia, (Z.Y., A.B. and R.K., the cold rolling, structural investigations and mechanical properties under project No. 14.578.21.0069, ID No. RFMEFI57814X0069); the Deutsche Forschungsgemeinschaft (DFG), Germany (C.H. and D.A.M., textural investigations within the Collaborative Research Centre (SFB) 761: “Steel – ab initio; quantum mechanics guided design of new Fe based materials”); the German Academic Exchange Service (Z.Y.,

financial support of her stay at the Institute of Physical Metallurgy and Metal Physics, RWTH Aachen University, Germany). The authors are grateful to the personnel of the Joint Research Centre, Belgorod State University, for their assistance with instrumental analysis.

References

[1] O. Grässel, L. Krüger, G. Frommeyer, L.W. Meyer, Int. J. Plast. 16 (2000) 1391–1409.
[2] G. Frommeyer, U. Brüx, P. Neumann, ISIJ Int. 43 (2003) 438–446.
[3] I. Gutierrez-Urrutia, D. Raabe, Acta Mater. 59 (2011) 6449–6462.
[4] H. Idrissi, K. Renard, D. Schryvers, P.J. Jacques, Scr. Mater. 63 (2010) 961–964.
[5] K. Jeong, J.-E. Jin, Y.-S. Jung, S. Kang, Y.-K. Lee, Acta Mater. 61 (2013) 3399–3410.
[6] T.S. Byun, Acta Mater. 51 (2003) 3063–3071.
[7] A. Dumay, J.-P. Chateau, S. Allain, S. Migot, O. Bouaziz, Mater. Sci. Eng. A 483–484 (2008) 184–187.
[8] O. Bouaziz, S. Allain, C.P. Scott, P. Cugy, D. Barbier, Curr. Opin. Solid State Mater. Sci. 15 (2011) 141–168.
[9] P. Kusakin, A. Belyakov, C. Haase, R. Kaibyshev, D.A. Molodov, Mater. Sci. Eng. A 617 (2014) 52–60.
[10] I.B. Timokhina, A. Medvedev, R. Lapovok, Mater. Sci. Eng. A 593 (2014) 163–169.
[11] E.G. Astafurova, M.S. Tukeeva, G.G. Maier, E.V. Melnikov, H.J. Maier, Mater. Sci. Eng. A 604 (2014) 166–175.
[12] N.K. Tewary, S.K. Ghosh, Supriya Bera, D. Chakrabarti, S. Chatterjee, Mater. Sci. Eng. A 615 (2014) 405–415.
[13] C. Haase, L.A. Barrales-Mora, D.A. Molodov, G. Gottstein, Metall. Mater. Trans. A 44A (2013) 4445–4449.
[14] C. Haase, L.A. Barrales-Mora, F. Roters, D.A. Molodov, G. Gottstein, Acta Mater. 80 (2014) 327–340.
[15] C. Haase, T. Ingendahl, O. Güvenç, M. Bambach, W. Bleck, D.A. Molodov, L. A. Barrales-Mora, Mater. Sci. Eng. A 649 (2016) 74–84.
[16] Y. Lü, D.A. Molodov, G. Gottstein, ISIJ Int. 51 (2011) 812–817.
[17] C. Haase, S.G. Chowdhury, L.A. Barrales-Mora, D.A. Molodov, G. Gottstein, Metall. Mater. Trans. A 44A (2013) 911–922.
[18] A.A. Saleh, C. Haase, E.V. Pereloma, D.A. Molodov, A.A. Gazder, Acta Mater. 70 (2014) 259–271.
[19] D.B. Williams, C.B. Carter, Transmission Electron Microscopy, Plenum Press, New York, 1996.
[20] R.E. Smallman, K.H. Westmacott, Philos. Mag. 2 (1957) 669–683.
[21] J. Hirsch, K. Lucke., Acta Met. Mater. 36 (1988) 2863–2882.
[22] J. Hirsch, K. Lucke, M. Hatherly., Acta Met. Mater. 36 (1988) 2905–2927.
[23] A. Belyakov, M. Murayama, Y. Sakai, K. Tsuzaki, M. Okubo, M. Eto, T. Kimura, J. Electron. Mater. 35 (2006) 2000–2008.
[24] C. Donadille, R. Valle, P. Dervin, R. Penelle, Acta Met. 37 (1989) 1547–1571.
[25] B.R. Kumar, M. Ghosh, Mater. Sci. Eng. A 457 (2007) 236–245.
[26] L. Bracke, K. Verbeken, L. Kestens, J. Penning, Acta Mater. 57 (2009) 1512–1524.
[27] R. Armstrong, I. Codd, R.M. Douthwaite, N.J. Petch, Philos. Mag. 7 (1962) 45–58.
[28] H. Mecking, U.F. Kocks, Acta Met. 29 (1981) 1865–1875.
[29] Y. Estrin, L.S. Toth, A. Molinari, Y. Brechet, Acta Mater. 46 (1998) 5509–5522.
[30] D.A. Hughes, N. Hansen, Acta Mater. 48 (2000) 2985–3004.
[31] N. Hansen, Scr. Mater. 51 (2004) 801–806.
[32] Z. Yanushkevich, A. Mogucheva, M. Tikhonova, A. Belyakov, R. Kaibyshev, Mater. Charact. 62 (2011) 432–437.
[33] F. Dalla Torre, R. Lapovok, J. Sandlin, P.F. Thomson, C.H.J. Davies, E.V. Pereloma, Acta Mater. 52 (2004) 4819–4832.
[34] R.Z. Valiev, Mater. Trans. 55 (2014) 13–18.
[35] M. Odnobokova, A. Belyakov, R. Kaibyshev, Metals 5 (2015) 656–668.
[36] P. Kusakin, A. Belyakov, R. Kaibyshev, D. Molodov, IOP Conf. Series: Mater. Sci. Eng. 63, 2014, art. no. 012059.
[37] M. Odnobokova, A. Belyakov, R. Kaibyshev, Adv. Eng. Mater. (2015), http://dx.doi.org/10.1002/adem.201500100.
[38] A. Belyakov, T. Sakai, H. Miura, R. Kaibyshev, Scr. Mater. 42 (2000) 319–325.
[39] A. Belyakov, Y. Kimura, Y. Adachi, K. Tsuzaki, Mater. Trans. 45 (2004) 2812–2821.
[40] M. Klimova, G. Dyakonov, S. Zherebtsov, G. Salishchev, D. Molodov, IOP Conf. Series: Mater. Sci. Eng. 63, 2014, art. no. 012157.